Redox state of the Neoarchean Earth environment

Aubrey L. Zerkle[1,2]*, Mark W. Claire[3,4], Shawn D. Domagal-Goldman[3,5], James Farquhar[1], and Simon W. Poulton[2]

[1]Department of Geology and ESSIC, University of Maryland, College Park, MD, USA

[2]School of Civil Engineering and Geosciences, Newcastle University, Drummond Building, Newcastle upon Tyne, NE1 7RU, UK

[3]Virtual Planetary Laboratory, University of Washington, Seattle, WA, USA

[4]School of Environmental Sciences, University of East Anglia, Norwich, UK

[5]NASA Headquarters, Washington, D.C., USA

Submitted to *Nature Geoscience*, 4 May, 2011

Resubmitted 28 October, 2011

*corresponding author: aubrey.zerkle@ncl.ac.uk

A Titan-like organic haze has been hypothesized for Earth's atmosphere prior to widespread surface oxygenation ~2.45 billion years ago (Ga). We present a high-resolution record of quadruple sulfur isotopes, carbon isotopes, and Fe speciation from the ~2.65-2.5 Ga Ghaap Group, South Africa, which suggest a linkage between organic haze and the biogeochemical cycling of carbon, sulfur, oxygen, and iron on the Archean Earth. These sediments provide evidence for oxygen production in microbial mats and localized oxygenation of surface waters. However, this oxygen production occurred under a reduced atmosphere which existed in multiple distinct redox states that correlate to changes in carbon and sulfur isotopes. The data are corroborated by photochemical model results that suggest bi-stable transitions between organic haze and haze-free atmospheric conditions in the Archean. These geochemical correlations also extend to other datasets, indicating that variations in the character of anomalous sulfur fractionation could provide insight into the role of carbon-bearing species in the reducing Archean atmosphere.

The Campbellrand-Malmani carbonate platform of the ~2.65-2.5 billion years old (Ga) Ghaap Group (Transvaal Supergroup, South Africa[1]) is one of the oldest carbonate platforms on Earth. Molybdenum concentrations and isotopes[2], Re/Mo ratios[3] and N isotope systematics[4] all suggest biological production of O_2 in surface waters during deposition of the upper part of the succession at ~2.5 Ga. This suggestion of significant O_2 production prior to Earth's first Great Oxidation Event[5] is supported by nutrient and trace metal systematics in coeval successions from other areas[6-9]. However, production of O_2 apparently did not lead to a pervasive rise in atmospheric oxygen levels[7].

Here, we focus on the lower part of the Ghaap Group, spanning the top of the Boomplaas Formation through the lower part of the Upper Nauga Formation (Fig. 1). Our samples come

from drillcore GKF01, and represent deposition primarily below wave base in a slope environment, with cyclic units of microbialites passing upwards into slope carbonates[1]. Radiometric age constraints place the base of the core at ~2.65 ± 0.08 Ga and the top of the measured section (within the Upper Nauga) at ~2.5 Ga[10]. The succession is exceptionally well-preserved, having experienced only gentle tectonic warping and sub-greenschist facies metamorphism[11].

Oxygenation of the Neoarchean oceans

Fe speciation analyses reflect water column redox conditions at the time of deposition, and show significant variations throughout the section (Fig. 1; Table S1). Many samples have elevated ratios of highly reactive Fe ($Fe_{carbonates} + Fe_{oxides} + Fe_{magnetite} + Fe_{pyrite}$) to total Fe ($Fe_{HR}/Fe_T > 0.38$), indicating deposition from an anoxic water column[12]. For those samples exhibiting high Fe_{HR}/Fe_T, the ratios of pyrite to highly reactive Fe (Fe_{Py}/Fe_{HR}) generally fall below 0.7-0.8, suggesting that when the bottom waters were anoxic, ferruginous (Fe(II)-rich) rather than euxinic (sulfide-rich) conditions were dominant[13]. Other samples representing shallow water deposition (microbialites of the Monteville Fm) or transported shallow-water deposits (the Lokammona), fall close to the average oxic Phanerozoic signal[12], suggesting formation from an oxic water column[13]. The low Fe_{HR}/Fe_T ratios and correlative facies assemblages imply that cyanobacterial O_2 production in microbial mats resulted in oxygenation of shallow surface waters as early as ~2.65 Ga.

Cyanobacterial oxygen production is further supported by trends in $\delta^{34}S$ and $\Delta^{33}S$. Sulfur isotope values for the majority of the section fall on or near a linear trend in $\delta^{34}S$ versus $\Delta^{33}S$ that has been described in Archean samples ($\Delta^{33}S = 0.9 \times \delta^{34}S$)[14] (Fig. 2A). This trend is interpreted to reflect mixing between sulfides formed from two primary atmospheric sources carrying

74 opposite sulfur mass independent fractionation (S-MIF) signals – e.g., an oxidized source
75 (sulfate) with negative $\Delta^{33}S$ and a zero valent source (S_8) with positive $\Delta^{33}S$. Samples associated
76 with microbial mats of the upper Monteville and the Lower Nauga have positive $\Delta^{33}S$ values that
77 plot parallel to the primary Archean array, but are enriched in ^{34}S by ~3 to 7‰ (Fig. 2A). This
78 trend could not result from changes in sulfate reduction fractionations alone, as this scenario
79 would only rotate the array. We suggest this association reflects formation of pyrite from a
80 residual pool of sulfide generated within the microbial mats[15] that was partially oxidized via O_2
81 near the mat surface, enriching the sulfide in ^{34}S (see Supplementary Information, SI, for further
82 discussion).

83 **Redox state of the Neoarchean atmosphere**

84 Covariations in $\Delta^{33}S$, $\Delta^{36}S$, and carbon isotope data reveal an important connection
85 between the Neoarchean sulfur and carbon cycles. Quadruple sulfur isotope values vary
86 considerably upcore (Fig. 1; Table S2), but all show S-MIF signals reflecting photochemical
87 production[16] in an atmosphere devoid of significant O_2[17]. Samples from the Boomplaas and
88 Lokammona Formations form a linear array in $\Delta^{33}S$ versus $\Delta^{36}S$, with a slope in $\Delta^{36}S/\Delta^{33}S$ of
89 approximately -0.96 (Fig. 2B). This slope is close to the reference line defined by previous
90 measurements of Archean sulfide and sulfate minerals (~-0.9), and is also interpreted to reflect
91 mixing of sulfur from two or more atmospheric sources[16]. In several distinct intervals within the
92 overlying section, the samples preserve $\Delta^{33}S$ and $\Delta^{36}S$ values that form arrays rotating in a
93 clockwise manner, forming steeper slopes in $\Delta^{36}S/\Delta^{33}S$, approaching -1.5 (Fig. 2B). The data
94 preserve a continuum of $\Delta^{36}S/\Delta^{33}S$ slopes between ~-0.9 and -1.5, and extend to highly positive
95 $\Delta^{33}S$ regardless of $\Delta^{36}S/\Delta^{33}S$. Biological sulfur cycling can produce scatter in the $\Delta^{36}S$ intercept,
96 since sulfate reduction can affect $\Delta^{36}S$ much more than $\Delta^{33}S$[18] (Fig. S1). However, a rotation of

97 the arrays to different $\Delta^{36}S/\Delta^{33}S$ slopes instead implies a change in the nature of the primary S-
98 MIF signature, either due to a change in $\Delta^{36}S/\Delta^{33}S$ for a single atmospheric signal, or due to
99 variable amounts of mixing between two or more atmospheric sources with different $\Delta^{36}S/\Delta^{33}S$.
100 Samples with the greatest deviation in $\Delta^{36}S/\Delta^{33}S$ occur in three distinct zones, at around 1400 m,
101 1100 m, and 800 m depth in the core. These zones correspond to intervals exhibiting highly ^{13}C-
102 depleted organic matter, falling to $\delta^{13}Corg$ values lower than -40‰ (Fig. 1; Fig. S2). Negative
103 excursions in $\delta^{13}Corg$ are typically interpreted to reflect higher CH_4 fluxes and an increased
104 contribution of methanotrophic biomass to sedimentary organic matter. A significant amount of
105 methane oxidation (methanotrophy) in the modern oceans occurs anaerobically[19]; however,
106 Fe_{HR}/Fe_T ratios near Phanerozoic oxic values in some of the ^{13}C-depleted samples suggest that
107 methanotrophy could also have proceeded via O_2 (Fig. 1).
108 A closer examination of previously published Neoarchean sulfur isotope data reveals
109 similar correlations between changes in $\Delta^{36}S/\Delta^{33}S$ slope and $\delta^{13}Corg$ in ~2.5 Ga sections in
110 South Africa (the Gamohaan Formation) and in Western Australia (the Mount McRae Shale)[7]
111 (Fig. S3). Samples forming an array with $\Delta^{36}S/\Delta^{33}S$ of -1.5 have also been reported for the ~2.73
112 Ga Tumbiana Formation of the Fortescue Group of Western Australia[20], which preserves a large
113 global negative $\delta^{13}Corg$ excursion down to -60‰[21]. We suggest that the correlation between
114 negative $\delta^{13}Corg$ excursions and $\Delta^{36}S/\Delta^{33}S$ anomalies in two sections and over ~200 million
115 years implies a global connection between methane and variations in atmospheric S-MIF signals.
116 **Modeling the Neoarchean atmosphere and hypotheses for S-MIF production**
117 Interpreting the magnitude of S-MIF in the geologic record requires knowledge of the
118 production, transformation, and mass partitioning of atmospheric sulfur, as well as subsequent
119 biogeochemical pathways to sedimentation. Recently measured[22] absorption spectra for $^{32}SO_2$,

120 $^{33}SO_2$ and $^{34}SO_2$ help constrain S-MIF production by SO_2 photolysis and imply that changing
121 concentrations of UV absorbers[23] (such as organic haze[20,24] formed at high atmospheric
122 CH_4:CO_2) might influence the S-MIF signature. S-MIF from SO_2 photolysis could also be
123 supplemented by other mass-independent kinetic isotope effects[25-27], in reactions such as SO
124 photolysis, $S+S_2 \rightarrow S_3$, CS_2 photolysis[28,29], or the production/destruction of excited-state SO_2.
125 Generation of significant S-MIF via any reaction other than SO_2 photolysis remains hypothetical
126 but worthy of future research given that multiple source reactions might help explain the data[25].
127 S-MIF, once created, partitions into all atmospheric sulfur species, and requires the simultaneous
128 presence of two (or more) atmospheric exit channels for preservation[17]. Furthermore, these exit
129 channels vary as a function of atmospheric methane, oxygen, and sulfur concentrations[14,30], and
130 biogeochemical processes could further transform the signal prior to preservation in sedimentary
131 environments[31].

132 To evaluate these possible alternatives, we ran 1-D early Earth photochemical models
133 where we increased CH_4 concentrations until an organic haze formed. The model utilized here
134 advances similar studies[24,32] by analyzing hazy atmospheres after the evolution of oxygenic
135 photosynthesis. Furthermore, we consider the effect of fractal aggregate scattering by
136 hydrocarbon aerosols[33], and contrast with traditional Mie scattering results. We use these models
137 to explore how optical depth, reaction pathways, and sulfur exit channels vary as a function of
138 CH_4 concentration, and tie these atmospheric properties to candidate mechanisms for the
139 observed changes in $\Delta^{36}S/\Delta^{33}S$. Figures 3 and S8 show two sets of photochemical model
140 simulations, both varying CH_4 concentrations from 1 to 50,000 ppm, while holding CO_2
141 concentrations at 1% and ground-level O_2 concentrations at 10 ppb. The two simulations differ
142 only in their hydrocarbon particle scattering physics (see SI for a discussion of boundary

143 conditions, particle formation and scattering). For both fractal and Mie scattering cases, higher
144 CH_4 resulted in increasingly reduced atmospheres, as evidenced by decreasing OH
145 concentrations (Fig. 3A; S8A). Despite large volcanic SO_2 and H_2S fluxes, none of our model
146 atmospheres accumulated large enough concentrations of SO_2 or OCS to affect S-MIF (see SI for
147 additional discussion). The dominant contributors to opacity between 180 and 220 nm in our
148 haze-free models were CO_2 absorption and Rayleigh scattering. Prior to haze formation, most
149 photons longward of 200 nm reached the Earth surface.

150 Even when CH_4 is too low to promote haze formation (CH_4:CO_2 < 0.1), changes to CH_4
151 concentrations altered the redox chemistry and impacted S-MIF exit channels. Enhanced CH_4
152 concentrations alone do not affect S-MIF, as the CH_4 absorption spectrum does not overlap the
153 vibrational bands of SO_2 that give rise to S-MIF. Instead, increases in CH_4 provided the reducing
154 capacity to polymerize elemental sulfur, thus promoting aerosol S_8 as an exit channel.
155 Simultaneously, SO_2 replaced sulfate as the most oxidized exit channel (Fig. 3C; S8C),
156 implicating the SO_2/S_8 couple as carriers of opposite-sign S-MIF. Reaction rates for S_3
157 polymerization, excited state SO_2 formation and SO photolysis all increased with increasing CH_4
158 concentrations (Fig. 3B; S8B). If any of these reactions produces significant S-MIF, they could
159 modify the signal produced by SO_2 photolysis. Regardless of mechanism, we suggest this haze
160 free regime is the origin of the 0.9 Archean 'reference' slope in $\Delta^{36}S/\Delta^{33}S$.

161 At CH_4:CO_2 > 0.1, a hydrocarbon haze dramatically altered our model atmospheres. The
162 broadband absorption by this haze caused a drastic reduction in photochemical reactions, and
163 specifically a slowdown of the S cycle. In the fractal scattering case, SO_2 photolysis rates slowed
164 by nearly two orders of magnitude (Fig 3B), as photons shortward of 220 nm were scattered by
165 the stratospheric haze. By contrast, SO_2 photoexcitation to $^1SO_2$ (210-327 nm) and $^3SO_2$ (337-

166 385 nm) remained prevalent. There are two potential sources of S-MIF variation in this regime: a
167 changing ratio of SO_2 photolysis to photoexcitation, and opacity effects arising from fewer total
168 photons. Other pathways involving multiple S atoms, such as S_3 polymerization or SO-SO dimer
169 formation, became unfeasible in the photon-starved CH_4:CO_2 > 0.1 environment.

170 For 0.1 < CH_4:CO_2 < 0.2, haze-induced shielding led to counter-intuitive decreases in the
171 CH_4 fluxes needed to support increasing CH_4 concentrations. As atmospheric CH_4 rose the haze
172 thickened, decreasing both CH_4 photolysis and the formation of radicals that destroy CH_4. The
173 haze therefore diminished the photochemical sinks for CH_4 such that larger concentrations could
174 be maintained at lower CH_4 source fluxes. This would have made atmospheres with 0.1 <
175 CH_4:CO_2 < 0.2 unstable. If a biosphere produced enough CH_4 to reach CH_4:CO_2 > 0.1, a positive
176 feedback would have ensued, increasing CH_4 concentrations until CH_4:CO_2 = ~ 0.2, at which
177 point further increases in CH_4 concentrations would have required biologically unfeasible CH_4
178 fluxes (see details in SI).

179 In both simulations, atmospheres with CH_4:CO_2 > 0.2 are unsustainable. If organic
180 particles scatter light according to Mie theory, a thick haze could be prevented by a Gaian
181 climate/CH_4 feedback[24] on global glaciations[34]. If organic particles behave like fractal scatterers,
182 a thick haze would have formed a UV shield effective enough to shut down photochemical haze
183 production (see Fig. 3B and SI). In either case, we can place an upper limit of ~0.2 on the
184 atmospheric CH_4:CO_2 ratio.

185 In summary, there are two accessible, stable regimes in our photochemical simulations:
186 CH_4:CO_2 < 0.1, and CH_4:CO_2 ~ 0.2. In the first of these regimes, SO_2 photolysis was a major
187 source of S-MIF, although other potential S-MIF reactions proceeded rapidly enough to be
188 quantitatively relevant. The exit channels varied as a function of atmospheric redox state, and the

magnitude of S-MIF in a given exit species would be expected to vary inversely with the relative mass fraction. In the second regime, the atmospheric S cycle operated slowly due to haze-induced opacity that significantly decreased photolysis rates in the lower atmosphere. SO_2 photolysis remained a likely source of S-MIF, and the lower photon availability could have led to significantSO_2 isotopologue absorption effects. S-MIF from symmetry-dependent de-excitation of SO_2 also had the potential to be an important source of S-MIF in this regime. SO_2 became the dominant exit channel, so its S-MIF signature should trend to 0 by mass balance considerations, with correspondingly higher S-MIF magnitudes in the minor (by mass) exit channels. Transition between the first and second regimes could therefore induce changes in S-MIF source magnitudes, coupled with changes in the reservoirs by which S-MIF exits the atmosphere. If low δ^{13}Corg reflects periods of enhanced methane flux, a bi-stable atmospheric transition from haze-free (CH_4:CO_2 < 0.1) to thin haze (CH_4:CO_2 ≅ 0.2) could explain the $\Delta^{36}S/\Delta^{33}S$ slope changes in ancient sediments.

Consideration of these models along with the high-resolution geochemical dataset presented here points to a Neoarchean depositional environment that includes: (1) microbial mat ecosystems similar to modern mats, with intensive internal recycling of sulfur; (2) cyanobacterial oxygen production and shallow water oxygenation as early as ~2.65 Ga; and (3) a link between methanotrophy and S-MIF producing atmospheric chemistry, indicating a reducing atmosphere with multiple episodes of organic haze formation during periods of enhanced biological CH_4 production. These records provide crucial evidence for the biogeochemical production and fate of oxidants and reductants in the oceans and atmosphere during the critical period in Earth history immediately pre-dating the first major rise in atmospheric oxygen.

Methods

Pyrite sulfur isotope compositions were determined on Ag_2S precipitates from distillation with chromous chloride. Quadruple S isotope measurements were performed at the University of Maryland, following the techniques described in Domagal-Goldman *et al.*[24], and reported as $\delta^{34}S = (({}^{34}S/{}^{32}S)_{sample}/({}^{34}S/{}^{32}S)_{V\text{-}CDT} - 1)$, $\Delta^{33}S = ({}^{33}S/{}^{32}S)_{sample}/({}^{33}S/{}^{32}S)_{V\text{-}CDT}\text{-}[({}^{34}S/{}^{32}S)_{sample}/({}^{34}S/{}^{32}S)_{V\text{-}CDT}]^{0.515}$, $\Delta^{36}S = ({}^{36}S/{}^{32}S)_{sample}/({}^{36}S/{}^{32}S)_{V\text{-}CDT}\text{-}[({}^{34}S/{}^{32}S)_{sample}/({}^{34}S/{}^{32}S)_{V\text{-}CDT}]^{1.9}$, with values given in permil (‰). Analytical uncertainties on S isotope measurements, estimated from long-term reproducibility of Ag_2S fluorinations, are 0.14, 0.008, and 0.20 (1σ) for $\delta^{34}S$, $\Delta^{33}S$, and $\Delta^{36}S$, respectively. Iron speciation was determined at Newcastle University via the sequential extraction techniques of Poulton *et al.*[12,13]. Replicate extractions give an RSD of <5% for all extraction steps. Total organic carbon (TOC) was measured on a Leco analyzer after treatment with dilute 20% HCl to remove carbonate phases. Organic C isotopes were measured on acid-treated samples by EA-IRMS, reported as $\delta^{13}C = (({}^{13}C/{}^{12}C)_{sample}/({}^{13}C/{}^{12}C)_{VPDB} - 1)$ (‰). Replicate analyses (n = 6) of an internal standard ($\delta^{13}C_{org}$ = -26.43‰) gave an average value of -26.43 ± 0.06‰ (1σ) during the sample run.

The 1-D photochemical model derives from Zhanle *et al.*[30], but contains the organic carbon species and chemistry from Domagal-Goldman *et al.*[24], as well as their δ two-stream radiative transfer scheme. The model simultaneously solves photochemical production and loss for 74 species undergoing 392 reactions, including transport by eddy and molecular diffusion over a 100 km grid with 0.5 km grid spacing. We adopt the temperature, eddy diffusion, and water vapor profiles from Domagal-Goldman *et al.*[24], leaving all other parameterizations (rainout, lightning, diffusion-limited hydrogen escape, etc.) unchanged. The modern solar flux is

used, although sensitivity tests were run approximating the spectral character of the sun at 2.5 Ga. Further details, including boundary conditions, are given in the Supplementary Information.

Correspondence and requests for materials should be addressed to Aubrey L. Zerkle, aubrey.zerkle@ncl.ac.uk.

Acknowledgements

We thank J. Kirschvink, J. Grotzinger, A. Knoll and the Agouron Institute for organizing and funding the Agouron drilling project. We also thank Mark Thiemens and one anonymous reviewer for constructive comments on the manuscript. This study was funded by the NASA Exobiology Program and NASA Astrobiology Institute (A.L.Z. and J.F.). M.W.C and S.D.D-G. would like to acknowledge support from the NAI Virtual Planetary Laboratory and the NASA Postdoctoral Program.

Author Contributions

A.L.Z. performed sulfur isotope analyses and spearheaded the study, M.W.C. and S.D. D-G. developed and ran the atmospheric models, S.W.P. collected the samples and performed Fe speciation analyses. All authors contributed to data interpretation and manuscript preparation.

Competing Financial Interests

The authors declare no competing financial interests.

References

1. Schroder, S., Lacassie, J. P. & Beukes, N. J. Stratigraphic and geochemical framework of the Aguoron drill cores, Transvaal Supergroup (Neoarchean-Paleoproterozoic, South Africa). *South African Journal of Geology* **109**, 23-54 (2006).

2. Wille, M. *et al.* Evidence for a gradual rise of oxygen between 2.6 and 2.5 Ga from Mo isotopes and Re-PGE signatures in shales. *Geochimica et Cosmochimica Acta* **71**, 2417-2435, (2007).

3. Godfrey, L. V. & Falkowski, P. G. The cycling and redox state of nitrogen in the Archaean ocean. *Nature Geoscience* (2009).

4. Kendall, B. *et al.* Pervasive oxygenation along late Archean ocean margins. *Nature Geoscience* **3**, 647-652 (2010).

5. Holland, H. D. The oxygenation of the atmosphere and oceans. *Philosophical Transactions of the Royal Society B-Biological Sciences* **361**, 903-915 (2006).

6. Anbar, A. D. *et al.* A whiff of oxygen before the great oxidation event? *Geochimica et Cosmochimica Acta* **71**, A24-A24 (2007).

7. Kaufman, A. J. *et al.* Late Archean biospheric oxygenation and atmospheric evolution. *Science* **317**, 1900-1903 (2007).

8. Garvin, J., Buick, R., Anbar, A. D., Arnold, G. L. & Kaufman, A. J. Isotopic evidence for an aerobic nitrogen cycle in the latest Archean. *Science* **323**, 1045-1048 (2009).

9. Reinhard, C. T., Raiswell, R., Scott, C., Anbar, A. D. & Lyons, T. W. A late Archean sulfidic sea stimulated by early oxidative weathering of the continents. *Science* **326**, 713-716 (2009).

10. Altermann, W. & Nelson, D. R. Sedimentation rates, basin analysis and regional correlations of three Neoarchean and Paleoproterozoic sub-basins of the Kaapvaal Craton as inferred from precise U-Pb zircon ages from volcani-clastic sediments. *Sedimentary Geology* **120**, 225-256 (1998).

11. Miyano, T. & Beukes, N. J. Phase relations of the stilpnomelane, ferriannite, and riebekite in very low-grade metamorphosed iron formations. *Geological Society of South Africa Transactions* **87**, 111-124 (1984).

12. Poulton, S. W. & Raiswell, R. The low-temperature geochemical cycle of iron: From continental fluxes to marine sediment deposition. *American Journal of Science* **302**, 774-805 (2002).

13. Poulton, S. W. & Canfield, D. E. Ferruginous conditions: A dominant feature of the ocean through Earth's history. *Elements* **7**, 107-112 (2011).

14. Ono, S. *et al.* New insights into Archean sulfur cycle from mass-independent sulfur isotope records from the Hamersley Basin, Australia. *Earth and Planetary Science Letters* **213**, 15-30, (2003).

15. Canfield, D. E. & Des Marais, D. J. Aerobic sulfate reduction in microbial mats. *Science* **251**, 1471-1473 (1991).

16. Farquhar, J., Bao, H. M. & Thiemens, M. Atmospheric influence of Earth's earliest sulfur cycle. *Science* **289**, 756-758 (2000).

17. Pavlov, A. A. & Kasting, J. F. Mass-independent fractionation of sulfur isotopes in Archean sediments: Strong evidence for an anoxic Archean atmosphere. *Astrobiology* **2**, 27-41 (2002).

18. Ono, S., Wing, B., Johnston, D., Farquhar, J. & Rumble, D. Mass-dependent fractionation of quadruple stable sulfur isotope system as a new tracer of sulfur biogeochemical cycles. *Geochimica et Cosmochimica Acta* **70**, 2238-2252 (2006).

19. Hinrichs, K.-U. Microbial fixation of methane carbon at 2.7 Ga: Was an anaerobic mechanism possible? *Geochemistry Geophysics Geosystems* **3**, 1-10 (2002).

20. Thomazo, C., Ader, M., Farquhar, J. & Philippot, P. Methanotrophs regulated atmospheric sulfur isotope anomalies during the Mesoarchean (Tumbiana Formation, Western Australia). *Earth and Planetary Science Letters* **279**, 65-75 (2009).

21. Hayes, J. M. in *Early Life on Earth* Vol. 84 (ed S. Bengston) 200-236 (Columbia University Press, 1994).

22. Danielache, S. O., Eskebjerg, C., Johnson, M. S., Ueno, Y. & Yoshida, N. High-precision spectroscopy of ^{32}S, ^{33}S, and ^{34}S sulfur dioxide: Ultraviolet absorption cross sections and isotope effects. *Journal of Geophysical Research - Atmospheres* **113**, D17314 (2008).

23. Ueno, Y. *et al.* Geological sulfur isotopes indicated elevated OCS in the Archean atmsophere, solving faint young sun paradox. *Proceedings of the National Academy of Sciences of the United States of America* **106**, 14784-14789 (2009).

24. Domagal-Goldman, S. D., Kasting, J. F., Johnston, D. T. & Farquhar, J. Organic haze, glaciations and multiple sulfur isotopes in the Mid-Archean Era. *Earth and Planetary Science Letters* **269**, 29-40, (2008).

25. Farquhar, J., Savarino, J., Airieau, S. & Thiemens, M. H. Observation of wavelength-sensitive mass-independent sulfur isotope effects during SO_2 photolysis: Implications for the early atmosphere. *Journal of Geophysical Research-Planets* **106**, 32829-32839 (2001).

26. Farquhar, J. *et al.* Isotopic evidence for Mesoarchaean anoxia and changing atmospheric sulphur chemistry. *Nature* **449**, 706-709 (2007).

27. Masterson, A. L., Farquhar, J. & Wing, B. A. Sulfur mass-independent fractionation patterns in the broadband UV photolysis of sulfur dioxide: Pressure and third body effects. *Earth and Planetary Science Letters* **306**, 253-260 (2011).

28. Zmolek, P. *et al.* Large mass independent sulfur isotope fractionations during photopolymerization of (CS2)-C-12 and (CS2)-C-13. *Journal of Physical Chemistry A* **103**, 2477-2480 (1999).

29. Domagal-Goldman, S. D. *et al.* Using Biogenic Sulfur Gases as Remotely Detectable Biosignatures on Anoxic Planets. *Astrobiology* **11**, 419-441 (2011).

30. Zahnle, K., Claire, M. & Catling, D. The loss of mass-independent fractionation in sulfur due to a Palaeoproterozoic collapse of atmospheric methane. *Geobiology* **4**, 271-283, doi:10.1111/j.1472-4669.2006.00085.x (2006).

31. Halevy, I., Johnston, D. T. & Schrag, D. P. Explaining the structure of the Archean Mass-Independent Sulfur isotope record. *Science* **329**, 204-207 (2010).

32. Pavlov A. A., Kasting J. F. and Brown L. L. UV-shielding of NH3 and O2 by organic hazes in the Archean atmosphere. *Journal of Geophysical Research* **106**, 1-23. (2001)

33. Wolf, E. T. & Toon, O. B. Fractal organic hazes provided an ultraviolet shield for early Earth. *Science* **328**, 1266-1268 (2010).

34. Haqq-Misra, J. D., Domagal-Goldman, S. D., Kasting, P. J. & Kasting, J. F. A revised, hazy methane greenhouse for the Archean Earth. *Astrobiology* **8**, 1127-1137 (2008).

35. Ono, S. H., Kaufman, A. J., Farquhar, J., Sumner, D. Y. & Beukes, N. J. Lithofacies control on multiple-sulfur isotope records and Neoarchean sulfur cycles. *Precambrian Research* **169**, 58-67 (2009).

36. Fischer, W. W. *et al.* Isotopic constraints on the Late Archean carbon cycle from the Transvaal Supergroup along the western margin of the Kaapvaal Craton, South Africa. *Precambrian Research* **169**, 15-27 (2009).

Figure Legends

Figure 1. Lithologic and geochemical data for the bottom part of core GKF01, through ~2.65 to 2.5 Ga sediments of the Ghaap Group (lithologies from Schröder *et al.*[1]). Data include pyrite sulfur isotope values ($\delta^{34}S$, $\Delta^{33}S$, $\Delta^{36}S$, and $\Delta^{36}S/\Delta^{33}S_{dev}$, calculated as the absolute value of the deviation from a $\Delta^{36}S/\Delta^{33}S$ slope defined by the Boomplaas and Lokammona Formations), carbon isotopes of organic carbon ($\delta^{13}Corg$), and Fe speciation data (Tables S2 and S3). Symbols are defined in Figure 2. Grey circles are from Ono *et al.*[35], grey squares are from Kendall *et al.*[4], and grey diamonds are from Fischer *et al.*[36].

Figure 2. Cross-plots for quadruple sulfur isotopes from the GKF01 section. A. $\delta^{34}S$ versus $\Delta^{33}S$ values. The dotted line is the Archean reference line ($\Delta^{33}S = 0.89 \times \delta^{34}S$)[14]. B. $\Delta^{33}S$ versus $\Delta^{36}S$

values. The solid line represents a reference array with $\Delta^{36}S/\Delta^{33}S$ slope of -0.9, and the dotted line represents an array with a slope of -1.5.

Figure 3. Photochemical model results for fractal particles. Models were run with CO_2 fixed at 1% and ground-level CH_4 mixing ratios from $1x10^{-6}$ to 0.05, displayed as CH_4:CO_2 ratios. Shaded regions indicate unconverged solutions. A. Mixing ratios (solid lines, left axis) and fluxes (dashed lines, right axis). B. Photochemical reaction rates relative to the rate at CH_4:CO_2 = 10^{-4} (non-red lines, left axis). Effective optical depth at 200 nm (solid) and 550 nm (dashed) (red lines, right axis). C. Sulfur exit channels shown as fraction of total sulfur leaving the atmosphere. The dotted line is the sum of exit channels shown.

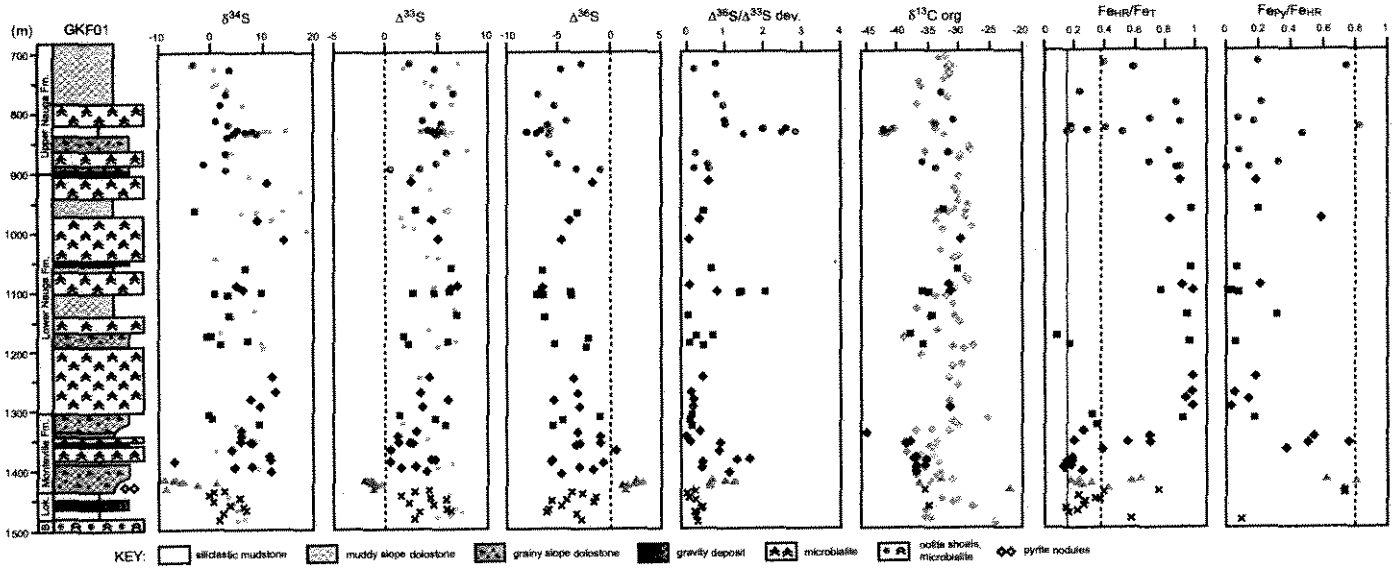

Figure 1. Zerkle et al.

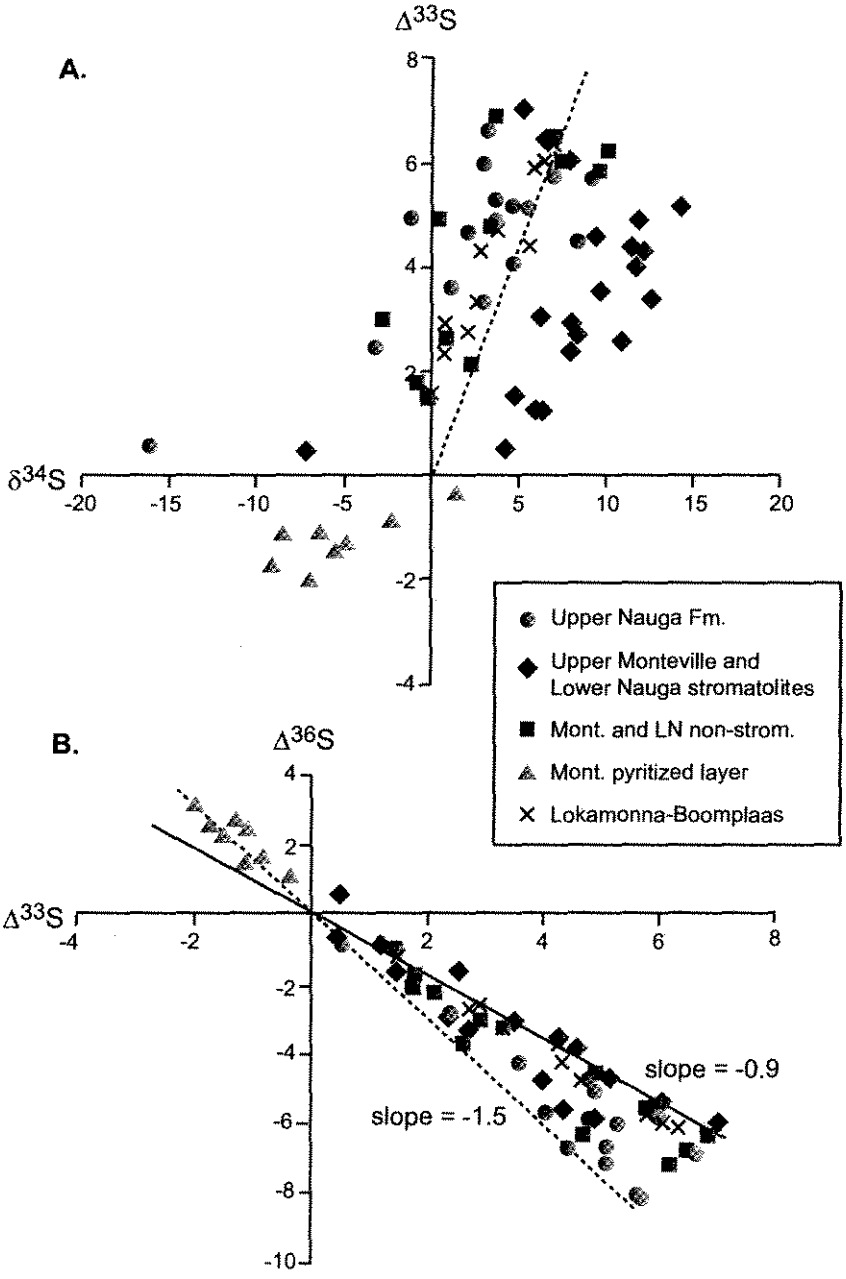

Figure 2. Zerkle et al.

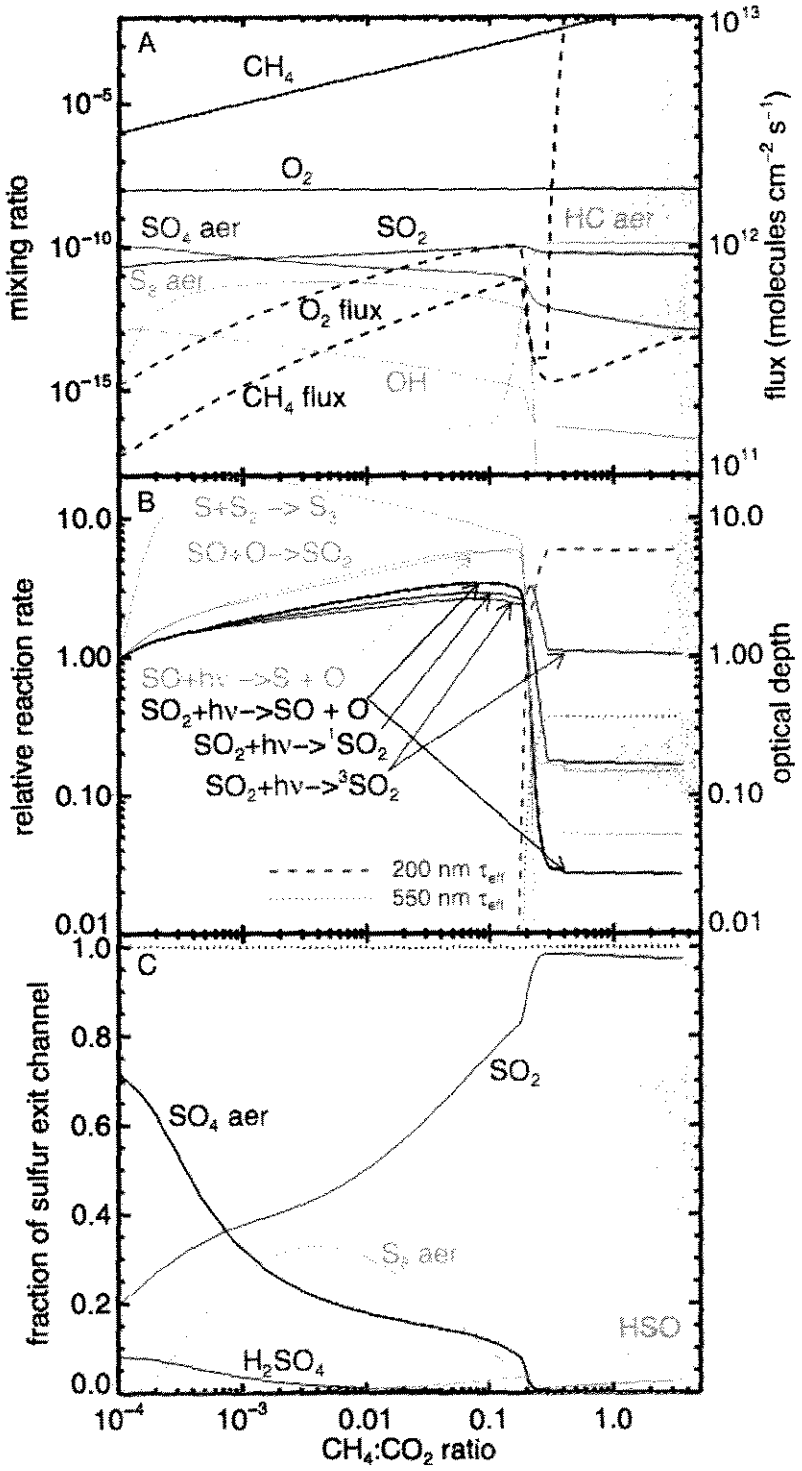

Figure 3. Zerkle et al.